The signal processing chain of the Low Frequency Aperture Array

Gianni Comoretto[a], Jader Monari[b], Carolina Belli[a], Simone Chiarucci[a], Francesco Schillirò[c], Marco Schiaffino[b], Federico Perini[b], Andrea Mattana[b], Monica Alderighi[d], Sergio d'Angelo[d], Sandro Pastore[e], Giovanni Naldi[b], Giuseppe Pupillo[b], Marco Poloni[b], Simone Rusticelli[b], Riccardo Chiello[f], Kris Zarb Adami[f], and Alessio Magro[g]

[a]INAF Osservatorio Astrofisico di Arcetri, Largo E. Fermi 5, Firenze, Italy
[b]INAF Istituto di Radioastronomia, Bologna, Italy
[c]INAF Osservatorio Astronomico di Catania, Catania, Italy
[d]INAF Istituto di Astrofisica Spaziale e Fisica Cosmica, Milano, Italy
[e]Sanitas EG, Milano, Italy
[f]University of Oxford, Phisics Department, oxford, United Kingdom
[g]University of Malta, La Valletta, Malta

ABSTRACT

The SKA LOW telescope is an interferometer composed of 512 stations. Each station consists of 256 electronically steered antennas. The Low Frequency Aperture Array is the portion of the SKA-LOW telescope including the antennas and the related electronics. The LFAA signal processing chain amplifies, transports and combines the signals from the antennas composing each station into a coherent beam. Beamforming is performed in the frequency domain, with stringent requirements on bandpass flatness, linearity in a RFI contaminated spectral region, and allowed signal degradation. We adopted an architecture including a highly optimized oversampled polyphase filterbank for channelization, and a distributed network beamformer. The system has been validated as part of the Aperture Array Verification System, a single station operating at the SKA site in Western Australia.

Keywords: SKA, Radio Astronomy, Digital Signal Processing, FPGA

1. INTRODUCTION

The SKA-LOW radio telescope[1] is an interferometric array of 512 stations, each composed of 256 dual-polarisation antennas, operating at frequencies between 50 and 350 MHz, for a total of 262,144 independent signal paths. It promises to be a transformational instrument for astrophysics in the coming decade,[2] due to its high sensitivity and wide frequency coverage.

The high sensitivity of the SKA telescope makes it vulnerable to radio frequency interferences, and requires a very stable and precise signal processing chain. The high number of signals to be processed require a very efficient implementation for this chain, in order to minimize costs and power usage.

The instrument sensitivity and very wide input band (1:7 fractional frequency ratio) are very challenging in term of RFI immunity. This is in part reduced by the very clean radio environment, but satellite, airborne or ducted radio broadcast signals are present. This poses strong constraints on the signal chain linearity and frequency selectivity. The RFI environment and linearity requirements are discussed in Sec. 2, and a mechanism to detect and flag impulsive RF signals is shown in Sec. 4.3.

Further author information: (Send correspondence to G.C.)
G.C.: E-mail: giovanni.comoretto@inaf.it
J.M: E-mail: jader.monari@inaf.it

Ground-based and Airborne Telescopes VIII, edited by Heather K. Marshall, Jason Spyromilio, Tomonori Usuda, Proc. of SPIE Vol. 11445, 1144571 · © 2020 SPIE
CCC code: 0277-786X/20/$21 · doi: 10.1117/12.2561699

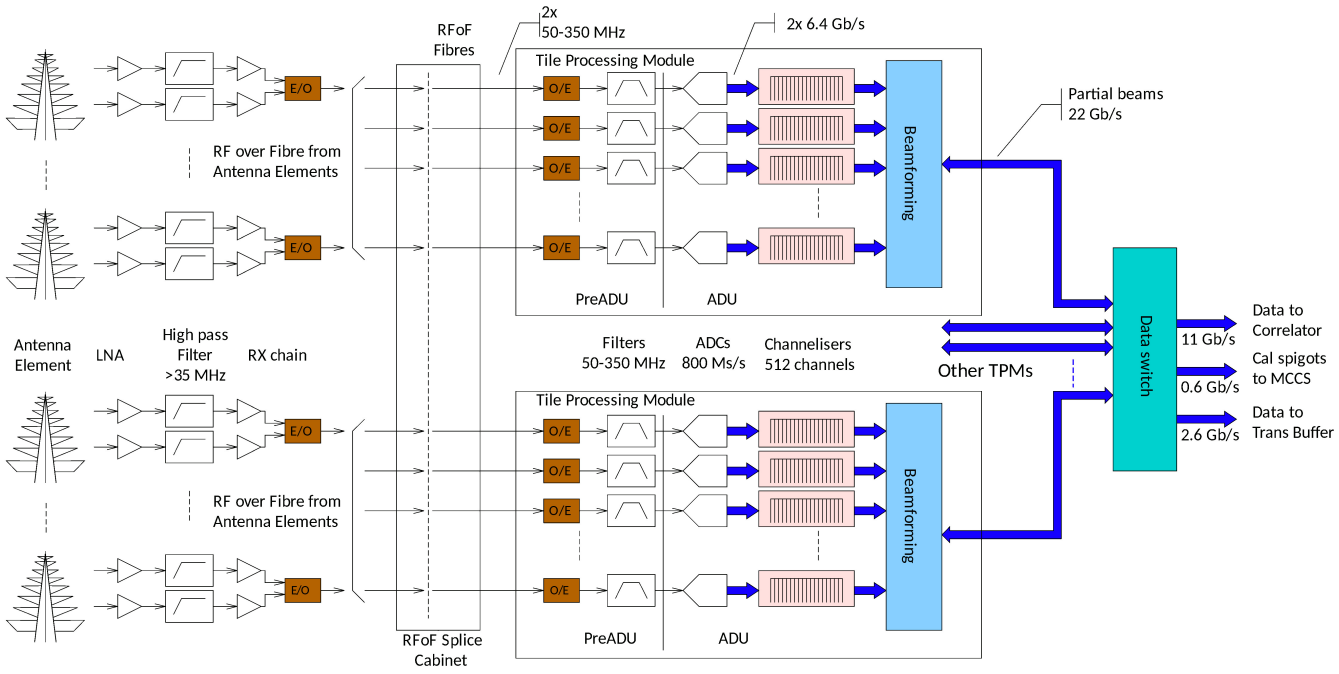

Figure 1. Block description of the LFAA signal processing chain

1.1 Low Frequency Aperture Array Architecture

The Low Frequency Aperture Array is the element of the telescope consisting of the antennas, the signal processing chain which groups them into stations and generate the station beams, and the related monitor, control and calibration computing infrastructure. Its general structure is shown in Fig. 1. The signal processing is based on the Italian Tile Processing Module (TPM) board. A first revision of the board[3] has been used in both versions of the Aperture Array Verification System, a demonstrative array at the SKA LOW site: AAVS1,[4] and the more recent AAVS2, composed of 256 antennas (Fig. 2). This has allowed characterization of the RFI environment, and to test the array operability in a realistic environment. A new revision of the board, with improved power performances,[5] will be used in the final system.

One TPM processes the signals for 16 antennas, both polarisations. 16 TPMs are connected together using 40 Gbps Ethernet links to implement a LFAA station. The TPM modules and supporting systems are hosted in a temperature controlled and shielded facility: the Central Processing Facility, for all the core stations, or Remote Processing Facilities, for stations in the array arms, to limit maximum fibre length around 4.5 km. The TPM is composed of an analog section (PreADU board), which receives, amplifies and conditions the antenna signals, and a digital section (ADU board) based on two Xilinx XCKU9P FPGAs, which converts them to digital streams, and performs the digital signal processing. A TPM is composed of one ADU board and two PreADU modules. A total of 8192 TPMs are required for the whole telescope.

The TPMs produce up to 48 beams from one station, trading bandwidth for number of beams. The total bandwidth summed over all beams is limited to 300 MHz. It also produces spigots of channelized samples from each antenna, to calibrate the station array, and a 2 bit copy of a portion of the beamformed data stream which is stored in a circular buffer for detection of fast radio transients.

The signal processing chain is controlled by the LFAA Monitor, Calibration and Control Subsystem (MCCS), which acquires these calibration spigots, compute the appropriate calibration coefficients for each antenna and the steering delays for beamforming, and in general controls the observation.

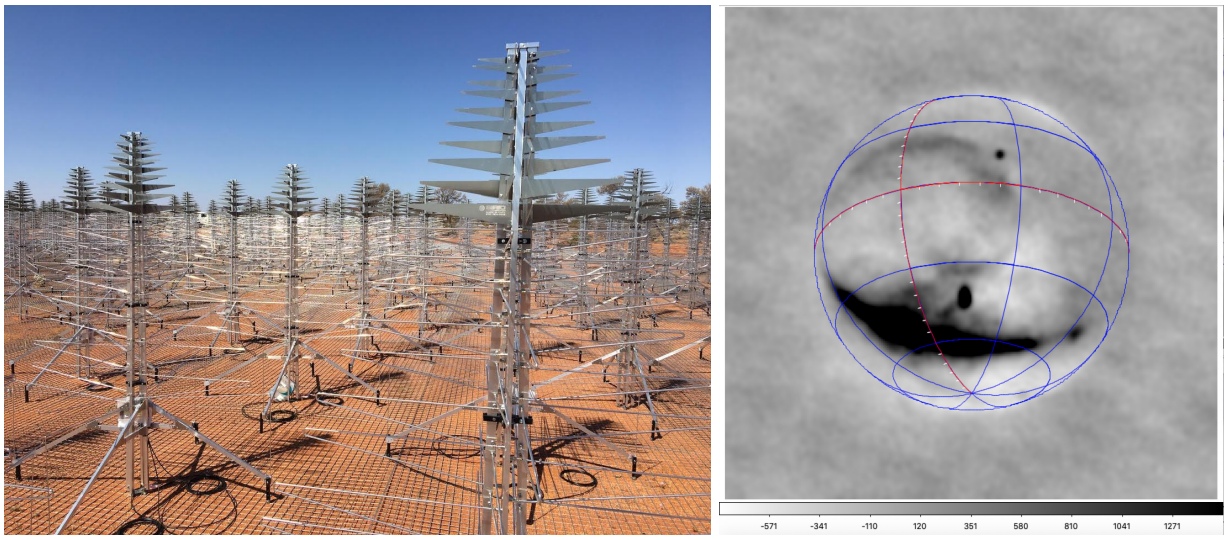

Figure 2. Antennas in the AAVS2 array (left) and example of a snapshot image at 160 MHz showing the Galactic emission and the Sun (right)

2. RADIO FREQUENCY INTERFERENCES

SKA-low is located in the RFI protected environment of the Murchison Radio Observatory, in Western Australia. Strict policies are enforced to limit self-induced RFI emissions, with most of the electronic equipment enclosed in a double shielded central facility room. The SKA LOW band is however heavily used for radio communication, and, especially, emissions from radio satellites are ubiquitous. The RFI environment has then been measured, and its spectrum used as a base for deriving the effects on SKA observations.

2.1 Radio Frequency Environment

The RFI environment has been analysed by a measurement campaign in the first months of 2019. Spectra of the signal collected by the individual antennas have been measured every few minutes, and a statistics of the spectral occupancy computed. An example of this analysis is shown in Fig. 3. For most of the time interfering signals are limited to the band between 240 and 270 MHz, to the FM broadcast band (88-108 MHz), and to a few other regions. Particularly relevant is the strong interference due to the Orbcom satellite constellation, around 138 MHz, and to aircraft audio communications, in the 120-140 MHz band. Occasional ducting events (1-2% of the time) propagate the FM band and digital TV signals in the 170-230 MHz band. In less than 0.1% of the time the RFI environment causes a complete saturation of the receiver chain. Some radar installations cause strong RFI below 20 MHz, but these are effectively filtered in the first stages of the receiver chain.

2.2 Linearity Requirements

A strong RFI not only contaminates the affected frequency region, but may show up as a weak signal in different bands, in a way that is difficult to discriminate from an astronomic spectral feature. SKA linearity requirements ask for no such features being visible up to 1000 hours of integration, with a frequency resolution of a few hundred Hz. This is in part relaxed by the beamforming directivity and by the intrinsic spatial smearing of a synthesis radiotelescope, but the telescope is sensitive enough to detect signals up to about -180 dBm on a single antenna.

Most of the non-linearities are due to second order intermodulation products. This poses a limit on the signal strength for any monochromatic RFI. A more complex model[6] has been used to estimate the analog chain nonlinearities up to the 3^{rd} order in the rich observed RFI spectrum. Results are shown in Fig. 4. The upper panel shows the assumed spectrum of the RFI signals (blue) and the resulting spectrum for the total nonlinear terms. The lower panel shows only the nonlinear terms, without the original RFI. The curves represent the limits for an input signal not to generate a significant 2^{nd} order harmonic (upper panel) and the sensitivity limits from the above requirement. The Orbcom signal is the most problematic interfering signal, generating

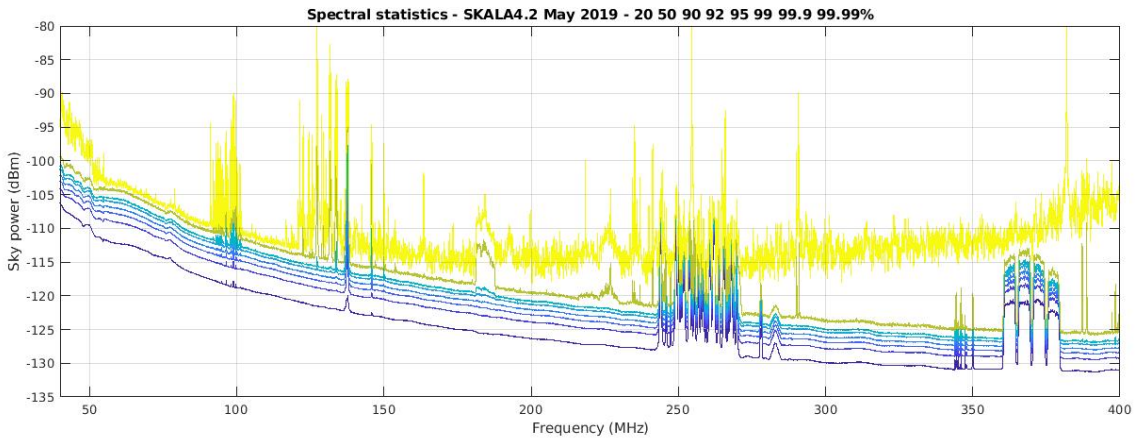

Figure 3. Statistics of the signal level for a typical LFAA antenna. Power is referred to a noise bandwidth of 10 kHz, at the antenna port. Blue lines represent percentiles from 20% to 99% (cyan), green and yellow lines represent upper 0.1% and 0.01% respectively

a strong second harmonic, but, as its frequency is extremely narrow, both the signal and the harmonic can be excised from the observed spectrum. Nonlinearity due to the ADC analog section have not been included in this analysis. The component specifications guarantee more than 80 dB of spurious free dynamic range and more than 90 dB of intermodulation product suppression for a signal close to the clipping level. As the input signal is noise-like, the amplitude of any harmonic component must be kept at least 10 dB below this level, further increasing suppression of nonlinear terms.

3. ANALOG PROCESSING

Analog elements include the receiver chain, the analog to digital converter, and the clock distribution tree. The nonlinearity and noise characteristics of the instrument are determined by these elements.

3.1 Receiver Chain

The analog receiver chain for LFAA performs the following functions:

- Amplifies the signal collected from each antenna to a level suitable to be converted to digital by the ADC.
- Filters the received band, to avoid aliasing on the high portion of the spectrum, and rejecting RFI below the band of interest.
- Transports the signal from the field node (station) to the digital equipment.

These functions are performed by the chain illustrated in Fig. 5. It is composed of the following elements:

- The antenna assembly consisting of dual-polarization antenna and two LNAs. The (multistage) LNA amplifies both polarisations by about 40 dB.
- The signal is transported over a short distance (∼10 metres) using a coaxial cable to a box (SMARTbox) containing the front-end modules (FEM) for 16 antennas. The FEM contains a high pass filter, with a cut-off frequency (-3dB) around 35 MHz, which helps rejecting the strong RFI below 50 MHz, the in-line Bias-T to feed the LNA power, an amplifier and the optical transmitter for the analog RFoF fibre link. The two polarization signals drive direct modulated laser diodes operating at 1270 nm and 1330 nm which are multiplexed onto a single optical fibre for each antenna and are routed from the Field Node to the processing electronics in a fiber-optic cable. A tone at 10 kHz is added to the laser current, to prevent oscillations in the laser cavity due to Rayelight backscattering in the fibre.

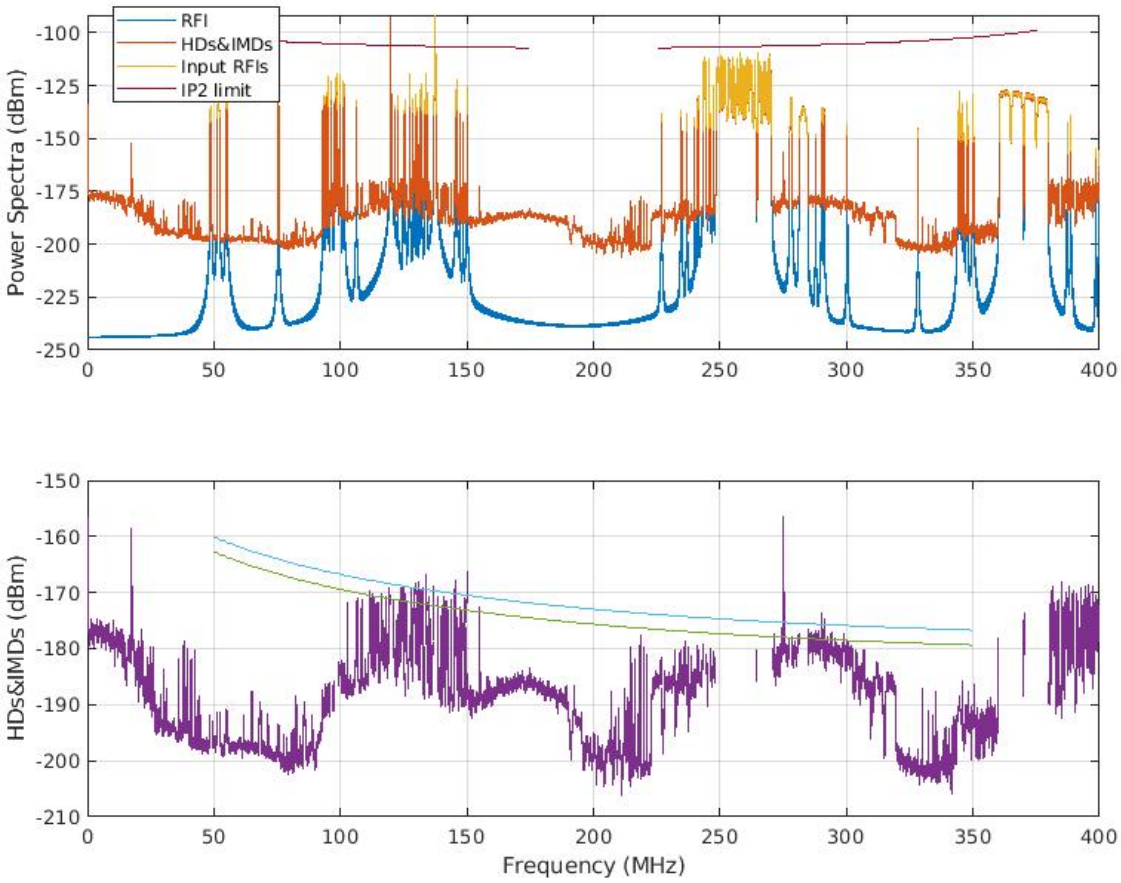

Figure 4. Upper curve: Intermodulation products and harmonic distortions terms (red) on the simulated input RFI spectrum (blue). The purple curve is the expected limit for RFI tones before significant second order harmonics becomes important. Lower curve: Resulting distortion terms alone. Smooth curves represent detectability limits in the observed spectrum, for the core stations alone (green) and for the whole LFAA array (blue).

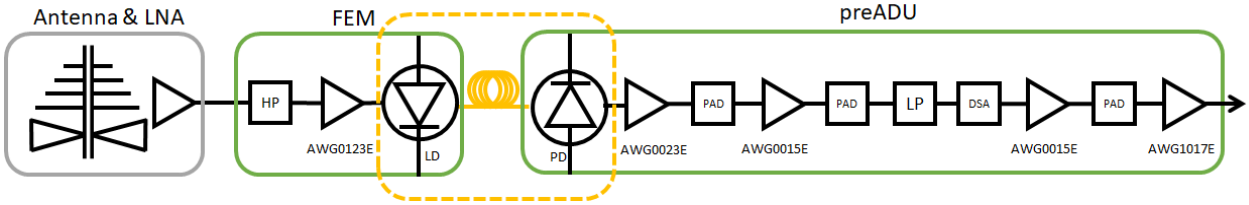

Figure 5. Analog receiver chain

- The fibre is routed to the processing facility in protected conduits, for thermal stability. At the processing facility, the optical fibre is connected to a pre-analog to digital unit (PreADU). The PreADU converts the optical signal back to electrical RF using a PIN photodiode receiver, performs low pass filtering for antialiasing and provides further amplification prior to the ADC. A digital step attenuator and final amplification stage set the correct levels to the acquisition system.

Principal parameters of the receiver chain are listed in Tab. 1. Nonlinearity parameters (OIP2, OIP3, 1 dB compression point) are referred to the output of the chain. The receiver noise temperature is 40 K for frequencies

Table 1. Parameters for the LFAA receiver chain

Total gain (100 MHz)	84	dB
Output level (typical)	-2.7	dBm
OIP2	49	dBm
OIP3	33	dBm
1 dB compression point	18	dBm
Noise temperature (150-350 MHz)	40	K

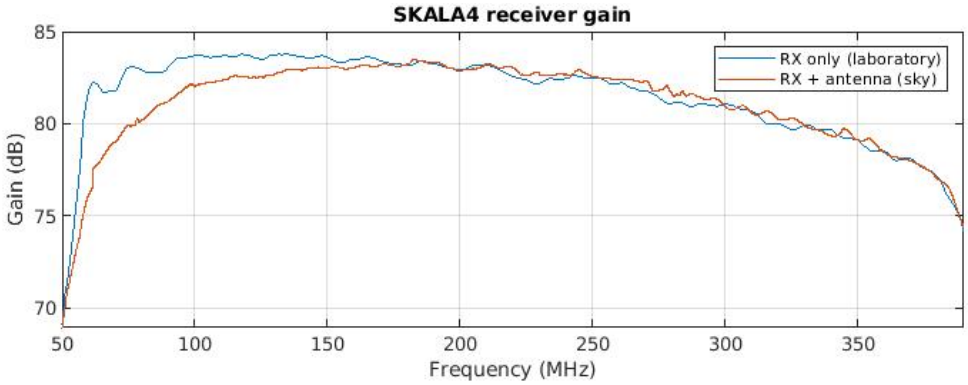

Figure 6. Total receiver chain gain as a function of frequency, as measured in laboratory (blue) and including the antenna gain, in the field (orange)

above 150 MHz, and increases to 100 K at 55 MHz. The total gain of the receiver chain is about 84 dB, with a sharp cutoff below 55 MHz due to the low pass filter and to the mismatch of the antenna to the first amplifier. This, together with the reduced antenna gain at low frequency, helps in rejecting the strong broadcast and radar signals ducted by the ionosphere below 30 MHz. The receiver bandpass is shown in Fig. 6. Blue curve is the gain for the standalone receiver, including the antenna mismatch as measured in the laboratory. Orange curve includes the antenna response, and has been derived by comparing the received signal in the field to the expected sky spectrum.

3.2 Analog to Digital Conversion

Antenna signals are digitized using an Analog Device AD9695 ADC. The device has 14 bit resolution, with a noise equivalent number of bits (ENOB of 10.9 bits, but only 8 bits are sent to the processing FPGA, due to bandwidth limitation. The ENOB of this configuration is above 7.9 bits. For a signal dominated by a Gaussian noise, the quantisation process is very linear for a signal RMS amplitude up to about 22% of the ADC clipping level, corresponding to 28-30 ADC units.

Noise contribution due to quantisation can be estimated analytically from the observed spectra at the site, and assuming an ENOB of 7.9 bits. Results are shown in Fig. 7, and are in good agreement with simulation work.[6] The added noise (SNR degradation) increases in general with frequency, as the quantisation noise has a flat spectrum while the sky signal has a steep negative spectral index, and depends on the RMS signal level at the ADC input. The optimal level has been set between 11 and 18 ADC units RMS, in order to leave some margin for transient RFI. The resulting maximum added noise is about 1% at 350 MHz and at an input level of 11 ADU.

3.3 Clock Stability

A stable clock is essential both for interferometric coherence and to achieve a high SNR. Clock jitter modulates any strong RF signal, scattering part of its power on nearby spectral regions, and increasing the noise floor. Low frequency clock jitter contributes to decorrelation. ADC clock is derived using an Analog Device AD9528 PLL, which specifies a clock jitter of -161 dBC/Hz above 10 kHz, corresponding to a jitter between 10 kHz and 800 MHz of 70 fs. Below 10 kHz the PLL copies the input clock jitter, which amounts to about 3 ps. The ADC itself

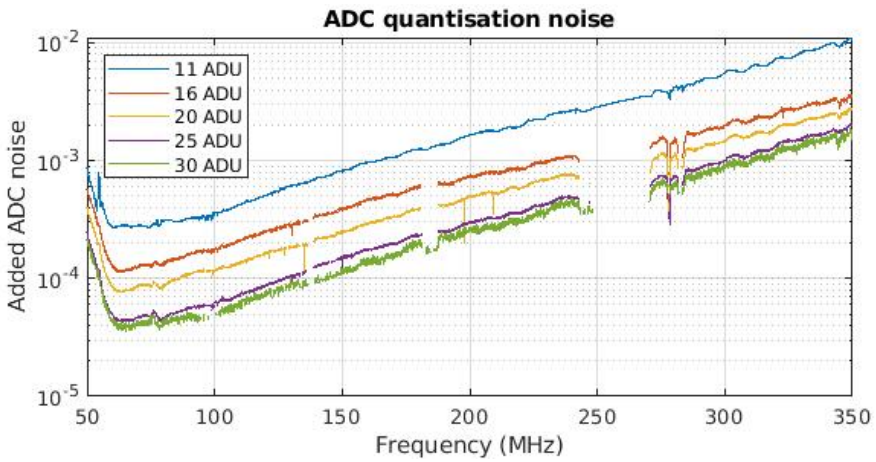

Figure 7. Added ADC quantisation noise for different signal levels, as derived from quantised spectra observed by the AAVS2 test array

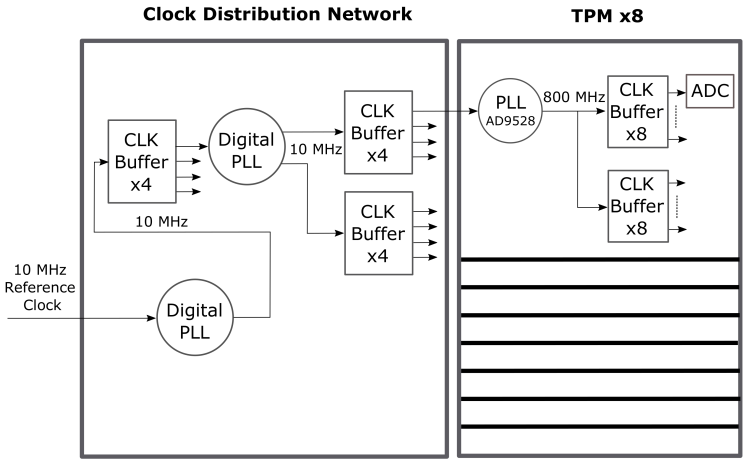

Figure 8. Clock distribution chain in the LFAA signal processing subsystem

has an internal clock jitter of 55 fs RMS. Inside the LFAA signal processing cabinets, clock is distributed using the structure shown in Fig. 8.

To validate the total jitter introduced by this structure, a high purity tone is digitized and a segment of 0.28 seconds is captured. The tone generator is locked to the 10 MHz standard used for the quantisation. The phase noise spectrum derived from these samples shows a white phase noise component, independent from the tone frequency, corresponding to 11 ENOB of quantisation noise, and an excess noise extending up to 10 MHz from the carrier frequency which translates to the total jitter shown in Fig. 9. Jitter is expressed in femtoseconds as a function of tone frequency. Blue and red lines are computed from the total phase noise in different integration bands, the yellow line includes a correction to remove the estimated quantisation noise. Measurements below 150 MHz are affected by the limited ADC accuracy. Phase noise below 240 Hz cannot be measured due to the limited acquisition time, but causes only a small line broadening at the highest spectral resolution (226 Hz) and a negligible interferometric decorrelation. The measured total jitter is around 300 fs over most of the band, increasing to 400 fs at the two extremes. Given the input signal spectrum, this jitter contributes to an extra noise of about 1% of the 8 bit quantisation noise.

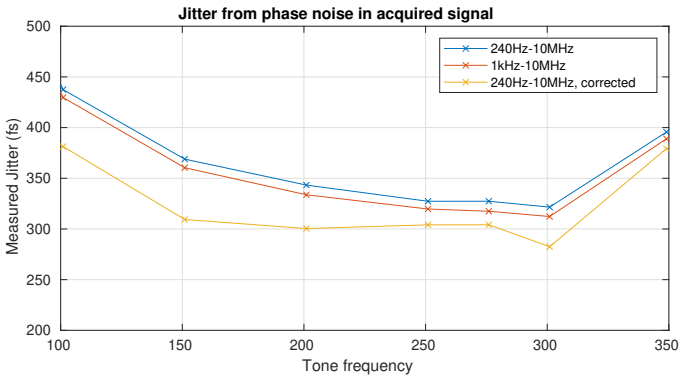

Figure 9. Jitter derived from the observed phase noise in an acquired high purity tone.

4. DIGITAL SIGNAL PROCESSING

The firmware structure implementing the TPM digital signal processing is described in Comoretto et al.[7] Beamforming is implemented in the spectral domain, by dividing the signal into channels spaced by 781.25 kHz and applying a phase term to each channel. Corresponding channels of different antennas composing a station are summed together and sent to the correlator. In spectral observations the individual channels are further channelised, up to a resolution of 226 Hz, and the resulting channels pasted together in a continuous spectrum. To avoid spectral holes, the beamformer channels are oversampled, for a total channel bandwidth of 923 kHz, and the overlapping portions of adjacent channels discarded. The channelisation allows an accurate frequency dependent calibration for each individual antenna.

4.1 Channeliser

The channeliser uses an oversampling polyphase filterbank architecture, as described by Harris.[8] This architecture is equivalent to an array of equally spaced down-converters followed by a low pass filter and a sample decimation, and is implemented with a single modified version of the filter operating directly on the sampled data, followed by a FFT. The channel spacing δf and the output sampling rate f_c are both an integer sub-multiple of the ADC sampling frequencies, but they do not need to be equal, and are usually in a small integer ratio. Channel passband (channel width) is set equal to δf. As $f_c > \delta_f$ it is possible to design the low pass filter with a flat response across the central δf part of the channel, and at the same time having a large rejection of any aliased copy of other channels. As shown in Fig. 10, the channel shape is chosen to be flat in the central part, equal to the channel spacing. The aliased image, due to the finite sampling rate and represented in red in the figure, folds back in the outer part of the channelized band, outside the channel width. Adjacent channels (in blue) have the flat portion of the response forming a contiguous region, without spectral holes.

The channeliser divides the input bandwidth into 512 channels with a spacing of 400/512 MHz, or 781.25 kHz, with an oversampling factor of 32/27. Thus each channel has a total band of 925.9 kHz, of which only the central

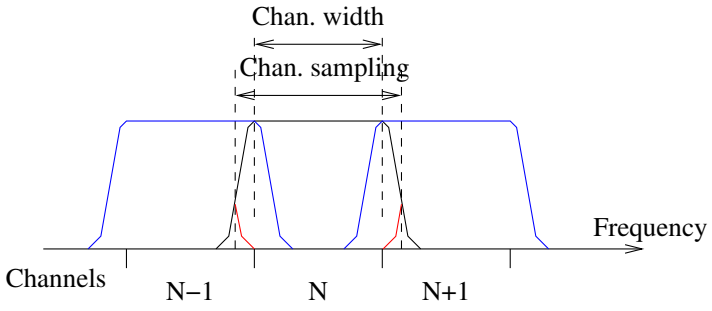

Figure 10. Channelization scheme using an oversampled filterbank. Red: aliased transition band, blue, adjacent channels.

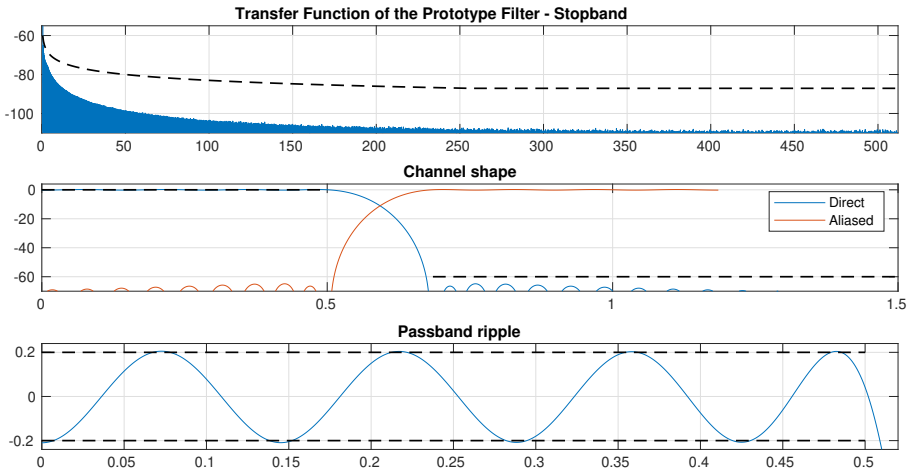

Figure 11. Theoretic filter response for the channelizer prototype filter

Table 2. Prototype filter parameters for the polyphase filterbank.

Passband edge	0.0004964
Stopband edge	0.0006645
Minimum attenuation	64 dB
Average attenuation	107 dB
Passband ripple	±0.2 dB
Number of taps N_f	16384

781.25 kHz are analyzed in the CSP. The implementation is highly optimized for the Xilinx architecture, in order to fit 16 independent channelisers in a single FPGA. The required channel response, due to the harsh RFI environment and the intrinsic all-sky sensitivity of the antennas, includes a very high stop-band rejection. In particular the Orbcom satellite carrier is present in the sky for most of the time, with a power level exceeding -100 dBm, and often reaching -90 dBm. The instrument can detect a narrow spectral line at a power level of -190 dBm, and thus a rejection of at least 90, preferably 100 dB is required to avoid an aliased copy of the line to be present in all LFAA channels. The prototype channeliser filter is based on a equiripple design, obtaining a good passband flatness and a high stop-band rejection, larger than 100 dB for most of the stop-band, with a limited number of filter taps. The channel response is shown in Fig. 11, with the principal parameters shown in Tab. 2.

Filter taps are rounded to integer values, with 18 bit accuracy. Various tests have been performed to determine the optimal coefficient scaling. Filter calculation is then performed using integer arithmetic. The final result is usually too large to be efficiently processed in subsequent stages, so it is rescaled and, rounded back to an integer value. Rescaling factor is 2^{-15}, giving a total average passband gain of the filter of 3.65, i.e. something less than 2 bits, producing an added noise that is 7% of that introduced in the ADC.

The FFT stage takes 1024 filtered, real samples and produce 512 complex channelized samples. The FFT engine operates at a oversampled rate, generating an output frame every 864 input samples, with an overlap of 160 samples between frames.

The FFT of a real valued signal is usually implemented in an optimized architecture, which places two samples in the real and imaginary components of the FFT input. These could be either two consecutive samples for the same signal, or the same sample from two signals. In this case a finite precision causes a spurious signal (aliasing) either between frequencies or, in the second case, between the same frequency in the two signals. The fixed point simulation can be used to evaluate these effects. We adopted an architecture with two consecutive samples in the

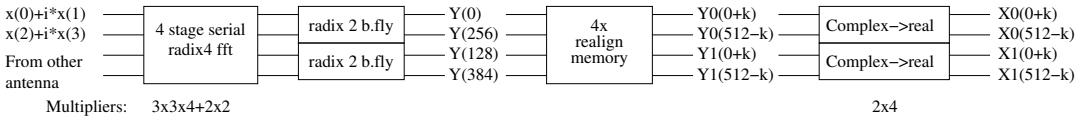

Figure 12. Structure of the FFT for real valued samples.

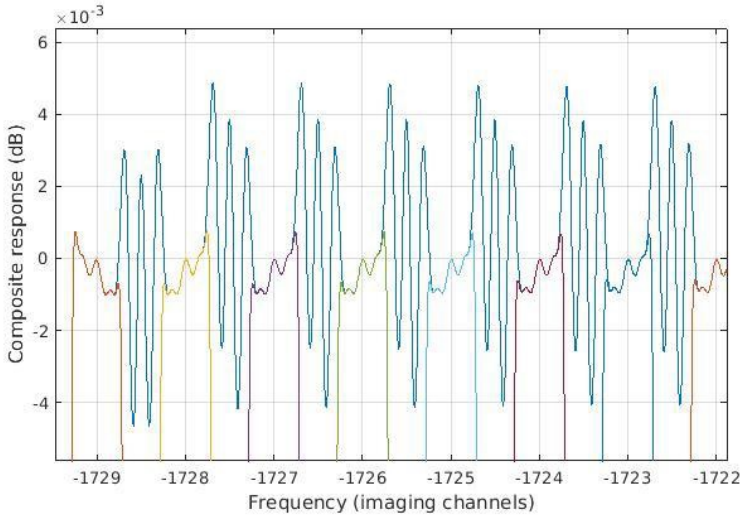

Figure 13. Cascaded response of the LFAA and correlator channelisers. First two channels shown are at the border between two LFAA channels. Colored curves represent individual correlator channels (226 Hz), blue curve the sum over adjacent channels

same complex value. This architecture is shown in Fig. 12. Both due to the possible presence of monochromatic RFIs and for the steep spectral index in the sky spectrum, the FFT output varies widely in amplitude. The FFT output is then rescaled using a variable coefficient, in the form of 2^{-k}, with k in the range from 1 to 8. The result is then rounded and represented using 12 bits.

The SKA telescope may operate in spectroscopic mode, with very high resolution, with a minimum channel spacing of 226 Hz. For this purpose each LFAA channel is further channelized in the correlator. In this way it is possible to compensate for the predictable passband shown in Fig. 13, obtaining an extremely flat filter response. The second stage channeliser uses a non oversampled polyphase filterbank architecture, with a Chebyshew filter design optimized in order to produce a constant integrated frequency response. This is shown in Fig. 13. Colored curves represent the response of individual channels, in a frequency region crossing two LFAA channels, and the blue curve the total response summed over adjacent channels. The latter varies by less than ± 0.05 dB, or $\pm 0.1\%$.

4.2 Calibration and beamforming

Before beamforming, the signals from each antenna are corrected for amplitude and phase instrumental response, for atmospheric propagation effects, and for beamforming tapering. Moreover, the signal is also equalized and normalized to a RMS amplitude appropriate for the quantisation performed in the data. *Calibration* in fact corresponds to two very different operations: a true calibration, based on an instrumental complex gain curve, determined externally, and an equalization, based on the actual measured signal amplitude. This latter is generated internally to the signal processing chain, and propagated downstream, to be removed in the data analysis.

The correction is expressed by a complex polarization matrix for each frequency channel, antenna and beam. The calibration coefficients are assumed to be $16 + 16$ bit complex values, and include

- The complex bandpass correction, to compensate for any instrumental effect

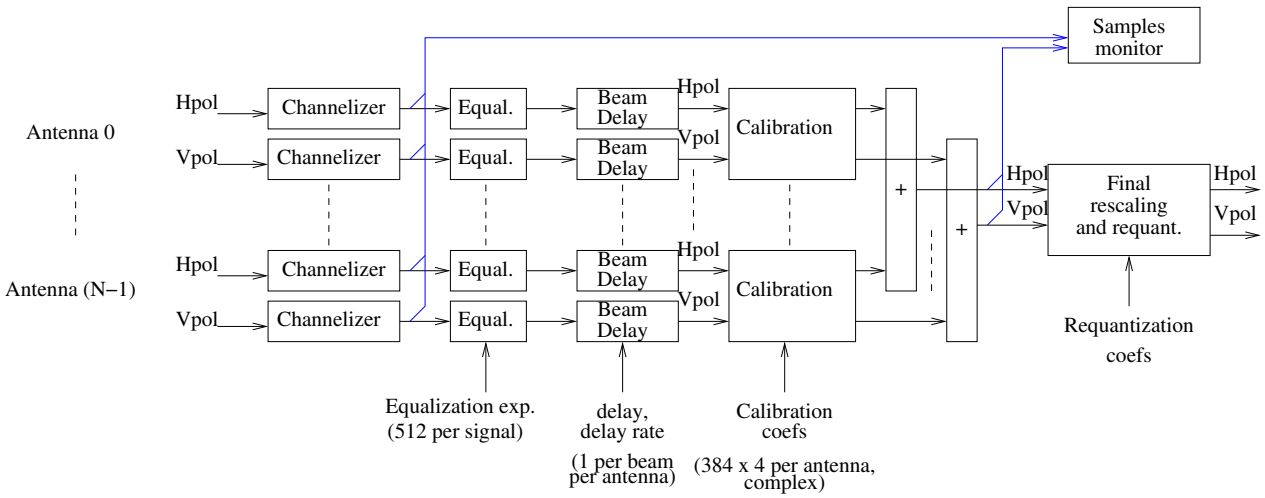

Figure 14. Calibration sequence in the channeliser and tile beamformer.

- A phase correction from the ionospheric calibration
- The inverse of the Jones matrix for the receiver
- A rotation of the polarization plane, to optionally compensate for parallactic angle rotation
- A further equalization factor, to bring the beamformed signal to the appropriate level for the final quantisation
- Antenna tapering for improving the station beam shape
- Optionally setting the calibration coefficient to zero disables a particular antenna (e.g. a faulty one) in the beamforming process.

Thus the beamformed signals $S(t, \nu, b)$ for one station, two polarisations, for the frequency channel ν and beam b is given by:

$$\begin{aligned} \begin{pmatrix} S_h(t,\nu,b) \\ S_v(t,\nu,b) \end{pmatrix} &= \sum_a \exp\left(2\pi j\, \nu\, \tau(t,a,b)\right) \begin{pmatrix} C_{hh}(\nu,a,b) & C_{hv}(\nu,a,b) \\ C_{vh}(\nu,a,b) & C_{vv}(\nu,a,b) \end{pmatrix} \begin{pmatrix} A_h(t,\nu,a) \\ A_v(t,\nu,a) \end{pmatrix} \\ \tau(t,a,b) &= \tau_0(a,b) + t\,\dot{\tau}(a,b) \end{aligned} \tag{1}$$

The beamformer takes each calibrated sample, corrects it with a phase corresponding to the delay contribution at the channel central frequency $\tau(t, a, b)$, and sums together the samples for all antennas.

The phase correction is computed multiplying the geometric delay by the channel frequency. The delay, in turn, is approximated using a linear function of time from an initial delay τ_0 and a delay slope $\dot{\tau}$. All these quantities (delay, delay slope, and phase) are expressed using integers, and thus introduce errors. Linear delay is updated using the delay slope every 1024 channelized samples (1105.92 μs).

These quantities, and all the calibration coefficients, are calculated externally to the TPM, and expressed as integer values. The matrix C is expressed as a complex mantissa, with $16 + 16$ bits of accuracy, and a 3 bit exponent specified every 8 frequency channels for each antenna.

The phase error, at the maximum frequency (350 MHz) and for an antenna at the station edge, is plotted in Fig. 15. The main effects are the jigsaw feature due to the finite step in the phase rotator, that cannot exactly follow the delay rate, and the curvature due to the delay acceleration. The decorrelation due to a phase error of a few milliradians is absolutely negligible, of the order of 10^{-6}.

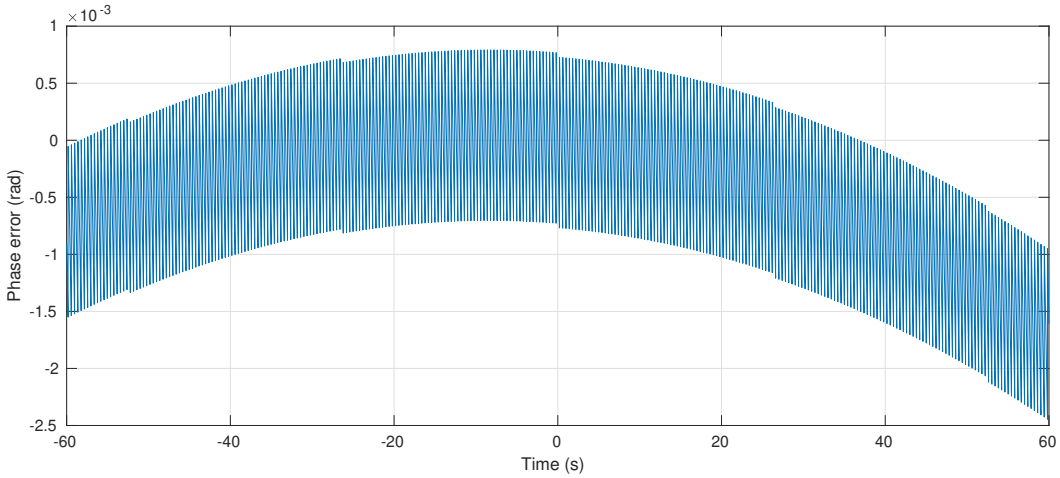

Figure 15. Phase error due to the quantisation in the delay model.

The jigsaw pattern produces a phase modulation, that in principle could generate harmonics of strong spectral lines. The modulation, however, occurs at a fundamental frequency of a few Hz, and the amplitude is sufficiently low to cause the first sideband to be attenuated of about 70 dB with respect to the modulated tone. The final effect is a slight broadening of strong interfering monochromatic tones, that could affect up to a few hundred Hz. As the spectral purity of RFI tones is much worse than this, the effect is absolutely irrelevant. The phase modulation causes also some excess noise, that is however of the order of -60 dB.

The delay can be specified for up to 48 independent sky positions. Each beam has a bandwidth equal a multiple of 6.25 MHz placed anywhere in the SKA LOW received band, for a total, summed over all beams, of 300 MHz. Setting some calibration coefficients to zero it is possible to implement separate sub-stations, i.e. aperture arrays of a subset of the 256 antennas, with a very flexible trade between beams, sub-stations, and bandwidth.

4.3 RFI Flagging Mechanisms

As seen in Sec. 2.1, we can include in our analysis three main types of RFIs:

- RFI that is persistent on the time scales of 1 second or more such as satellites, ducted broadcast emission and airplane communications.
- Transient RFI on time scales less than 1 second such as lightning.
- Narrow band RFI which is normally due to leakage of clock internal to the telescope (bandwidth much less than the resolution bandwidth).

Finally, clipping that may occur with LFAA processing, may be considered as a fourth type of RFI. When the signal representation is reduced (mainly at the output of the LFAA and before correlation), the signal may be clipped if its value exceeds the representable range. This also may cause flagging. It should be noted that flagging and clipping are two different concepts. Samples may be flagged, clipped or both, but clipping does not imply flagging and flagging does not require clipping. In LFAA occasional clipping is allowed, as flagged samples may affect long segments of correlated data.

Mechanisms to detect potential RFI situations operate mainly on signal level, detecting when this level increases to a point when nonlinear effects become likely. Affected samples are destructively marked, using a special value not used for valid samples. In LFAA the signal processing chain detects and flags RFI signals using four strategies, as shown in Fig 16.

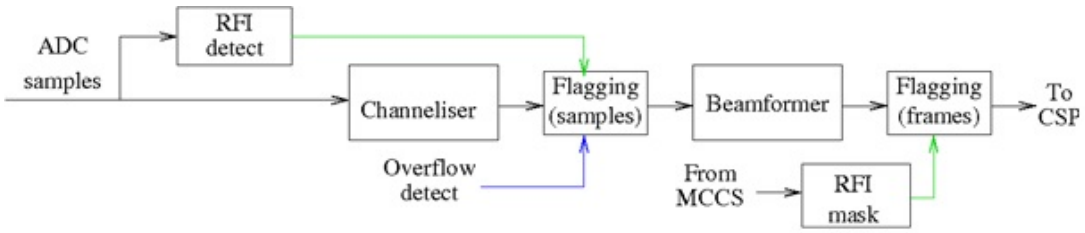

Figure 16. Flagging mechanism in LFAA. If increase in power is detected in a block of ADC samples, the corresponding channelised samples are flagged. Channeliser also flags samples which exceed allowed range .

1. Before channelisation, the wideband signal power level is tested for a sudden increase on a timescale of a few channelised samples (1.08μs), compared to the power averaged on a longer timescale (milliseconds to seconds). This is indicative of pulsed radio signals (e.g. radar, or lightning). The flagging threshold, and the averaging time for the shorter and longer timescales are selected by the MCCS. Flagging occurs on channelised samples, which are set to the most negative value (e.g. -128 for 8 bit). Total power measurement is performed on blocks of 864 ADC samples (corresponding to 1 channelised sample). Flagging is propagated across the channeliser and applied to the corresponding channelised samples.

2. After channelisation, LFAA channels that saturate with respect to the pre-set quantisation range are flagged. The quantisation range is set on a per-channel basis, and saturation is indicative of very high, narrow-band signals. Saturation is detected also in the final requantisation of beamformed samples to 8 bits, before sending them to CSP.

3. At the output of the beamformer, flagging the channelised data segments sent to the CSP when a pulsed RFI with timescales of the order of 1 ms is detected.

4. The MCCS can provide a per-channel RFI mask for each station. The mask is specified with a coarse time resolution (minutes), based on a priori information (e.g. satellite transit times), or using the results from the calibration and autocorrelation spectra. The mechanism is useful if the mask is specified to a resolution (in frequency, time or both) better than that of the visibilities transmitted to SDP.

In Fig. 17 the details of the first flagging mechanism is shown. A long term (milliseconds to seconds) moving average of the ADC power level is computed in a long term accumulator, using an infinite impulse response (IIR) filter. A short term accumulator integrates the total power over blocks of M (typically 864) samples, corresponding to one channelised sample. These are further averaged over two consecutive frames to have a more time-invariant response of the detector. When the short term power level exceeds the long term level by a programmable threshold, a RFI flag is generated. Flagging occurs at channelised sample rate, and affects channelised samples with a programmable pre-event and post-event margin, to include the finite response (ringing) of the channeliser filter. The flagging threshold, and the averaging time for the shorter and longer timescales are selected by the MCCS.

5. CONCLUSIONS

The signal chain for the Low Frequency Aperture Array provides a flexible and powerful frequency domain beamformer. It allows calibration of each individual antenna, and implements up to 48 separate beams, and/or substations, with a total processed bandwidth of 300 MHz. Its innovative design for an oversampling channeliser allows for a seamless reconstruction of the observed band, with a spectral fidelity better than 0.1%, and can be easily adopted in any channelization system with a very large (up to 10^7) number of channels. The efficient design is implemented using a relatively small FPGA, with a total of 110 hard multipliers used to filter, calibrate and beamform each input signal. The system linearity has been particularly cared for, both in the analog and digital sections, to minimize the effects of RFI signals.

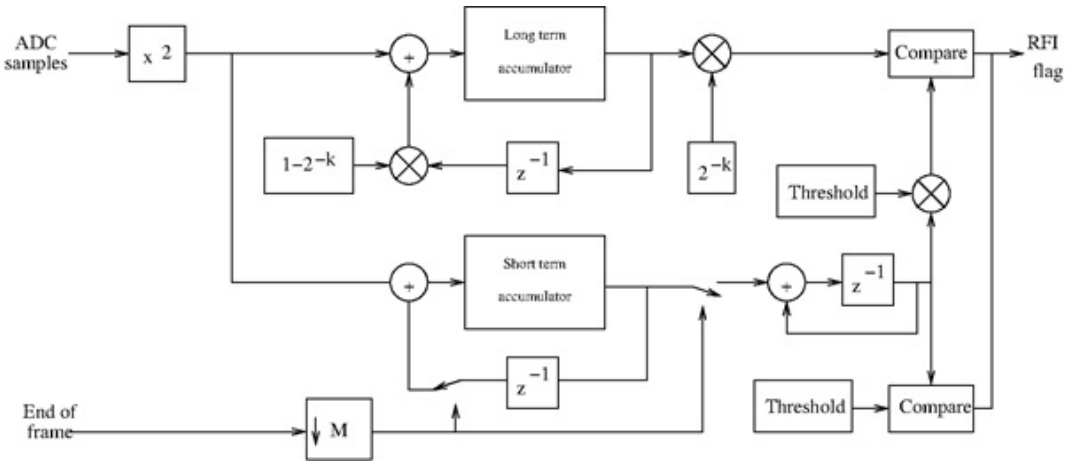

Figure 17. LFAA broadband RFI detector. Flagging occurs when total power measured on short term interval (864 samples) exceeds long term average level by a programmable threshold.

REFERENCES

[1] Dewdney, P., "Ska1 system baseline design v2," Tech. Rep. SKA-TEL-SKO-0000002, SKA Organisation (2016).

[2] Braun, R., Bourke, T., Green, J. A., Keane, E., and Wagg, J., "Advancing Astrophysics with the Square Kilometre Array," in [*Advancing Astrophysics with the Square Kilometre Array (AASKA14)*], 174 (Apr 2015).

[3] Naldi, G., Mattana, A., Pastore, S., Alderighi, M., Zarb Adami, K., Schillirò, F., Aminaei, A., Baker, J., Belli, C., Comoretto, G., Chiarucci, S., Chiello, R., D'Angelo, S., Dalle Mura, G., De Marco, A., Halsall, R., Magro, A., Monari, J., Roberts, M., Perini, F., Poloni, M., Pupillo, G., Rusticelli, S., Schiaffino, M., and Zaccaro, E., "The Digital Signal Processing Platform for the Low Frequency Aperture Array: Preliminary Results on the Data Acquisition Unit," *Journal of Astronomical Instrumentation* **6**, 1641014 (Mar 2017).

[4] Benthem, P., Gerbers, M., Bij de Vaate, J.G., Wynholds, S., Bast, J., Booler, T., Colgate, T., Crosse, B., Emrich, D., Hall, P., Juswardy, B., Kerniey, D., Schlagenhaufer, F., Sokolowski, M., Sutinjo, A., Ung, D., Wayth, R., Williams, A., Alderighi, M., Bolli, P., Comoretto, G., Mattana, A., Monari, J., Naldi, G., Perini, F., Pupillo, G., Rusticelli, S., Schiaffino, M., Schillirò, F., Aminei, A., Chiello, R., Jones, M., Baker, J., Bennett, R., Halsall, R., Kaligeridou, G., Matthews, R., Schnetler, H., Abraham, J., De Lera Acedo, E., Faulkner, A., Razavi- Ghods N., Cutajar, D, DeMarco, A., Magro, A., and Zarb Adami, K., "The low frequency receivers for ska 1-low: Design and verification," in [*2017 XXXIInd General Assembly and Scientific Symposium of the International Union of Radio Science (URSI GASS)*], IEEE (Aug 2017).

[5] Schillirò, F., Alderighi, M., Belli, C., Chiarucci, S., Chiello, R., Comoretto, G., D'Angelo, S., Magro, A., Mattana, A., Monari, J., Naldi, G., Pastore, S., Perini, F., Poloni, M., Rusticelli, S., Schiaffino, M., and Zarb Adami, K., "Design and prototyping of the italian tile processing module for the low frequency aperture array deployment," in [*Ground-based and Airborne Instrumentation for Astronomy VIII*], International Society for Optics and Photonics, SPIE (Dec 2020).

[6] Chiarucci, S. and Comoretto, G., "An end-to-end model for the correlator and beamformer of the square kilometer array low frequency aperture array," in [*Ground-based and Airborne Instrumentation for Astronomy VIII*], International Society for Optics and Photonics, SPIE (Dec 2020).

[7] Comoretto, G., Chiello, R., Roberts, M., Halsall, R., Adami, K. Z., Alderighi, M., Aminaei, A., Baker, J., Belli, C., Chiarucci, S., D'Angelo, S., De Marco, A., Mura, G. D., Magro, A., Mattana, A., Monari, J., Naldi, G., Pastore, S., Perini, F., Poloni, M., Pupillo, G., Rusticelli, S., Schiaffino, M., Schillirò, F., and Zaccaro, E., "The Signal Processing Firmware for the Low Frequency Aperture Array," *Journal of Astronomical Instrumentation* **6**, 1641015 (Mar 2017).

[8] Harris, F. J., Dick, C., and Rice, M., "Digital receivers and transmitters using polyphase filter banks for wireless communications," *IEEE Transactions on Microwave Theory and Techniques* **51**(4), 1395–1412 (2003).